


# High-power single mode GaSb-based $2\ \mu\text{m}$ superluminescent diode with double-pass gain

Cite as: Appl. Phys. Lett. **115**, 231106 (2019); <https://doi.org/10.1063/1.5127407>

Submitted: 11 September 2019 . Accepted: 23 November 2019 . Published Online: 05 December 2019

Nouman Zia, Jukka Viheriälä, Eero Koivusalo, and Mircea Guina

## COLLECTIONS

 This paper was selected as Featured



View Online



Export Citation



CrossMark

## ARTICLES YOU MAY BE INTERESTED IN

[BAIGaN alloys nearly lattice-matched to AlN for efficient UV LEDs](#)

Applied Physics Letters **115**, 231103 (2019); <https://doi.org/10.1063/1.5129387>

[Antireflection coating on organic nonlinear optical crystals using soft materials](#)

Applied Physics Letters **115**, 231107 (2019); <https://doi.org/10.1063/1.5126462>

[Deep learning optimized single-pixel LiDAR](#)

Applied Physics Letters **115**, 231101 (2019); <https://doi.org/10.1063/1.5128621>

Lock-in Amplifiers  
up to 600 MHz



Zurich  
Instruments



# High-power single mode GaSb-based $2\ \mu\text{m}$ superluminescent diode with double-pass gain

Cite as: Appl. Phys. Lett. **115**, 231106 (2019); doi: [10.1063/1.5127407](https://doi.org/10.1063/1.5127407)

Submitted: 11 September 2019 · Accepted: 23 November 2019 ·

Published Online: 5 December 2019



View Online



Export Citation



CrossMark

Nouman Zia,<sup>a)</sup> Jukka Viheriälä, Eero Koivusalo, and Mircea Guina

## AFFILIATIONS

Physics Units, Tampere University, Korkeakoulunkatu 3, 33720 Tampere, Finland

<sup>a)</sup> Author to whom correspondence should be addressed: [nouman.zia@tuni.fi](mailto:nouman.zia@tuni.fi)

## ABSTRACT

We report a broadband superluminescent diode operating around a  $2\ \mu\text{m}$  wavelength, optimized for high-power broadband operation. The high power operation is achieved by using a GaInSb/AlGaAsSb heterostructure positioned in a ridge waveguide with a J-shaped layout to form a double-pass geometry. To avoid lasing at high current while enabling high gain, a cavity suppression element is used. This combination allows demonstration of an output power as high as 120 mW for continuous-wave (CW) operation at room temperature, with a spectral full width at half maximum of about 43 nm. The maximum power spectral density was measured to be 1.8 mW/nm, which is about a fourfold increase compared to the state-of-the-art results for this wavelength range. To avoid heating, the diode was also driven with low duty-cycle current pulses; in this case, a peak power of more than 300 mW was achieved without any sign of roll-over (power was limited by the current injected). For CW operation, the central emission wavelength could be tuned by current injection between 1900 nm at 200 mA and 2027 nm at 2000 mA. Devices produce a Gaussian output beam that is suitable for coupling to single mode waveguides.

© 2019 Author(s). All article content, except where otherwise noted, is licensed under a Creative Commons Attribution (CC BY) license (<http://creativecommons.org/licenses/by/4.0/>). <https://doi.org/10.1063/1.5127407>

Light sources emitting around  $2\text{--}3\ \mu\text{m}$  are particularly useful for spectroscopic sensing due to the strong molecular absorption of several important gases.<sup>1</sup> This wavelength range is, for example, used for the detection of CO,<sup>2</sup> CO<sub>2</sub>,<sup>3</sup> NH<sub>3</sub>,<sup>3</sup> and N<sub>2</sub>O<sup>4</sup> and *in situ* combustion and temperature sensing.<sup>5</sup> These applications would require a compact, power efficient, high power, and high brightness light source, which is wavelength tunable for multiple gas sensing. A semiconductor laser source is the ideal candidate due to its compactness, power efficiency, and low cost. However, a traditional semiconductor laser for spectroscopy has a very narrow tuning range,<sup>6</sup> which makes it unfit for multiple gas sensing and wide tuning spectroscopy. To this end, a wide spectral tuning can be achieved by using laser arrays,<sup>7</sup> Vernier-effect,<sup>8</sup> table-top external cavity lasers,<sup>9</sup> etc. The above-mentioned technologies are either not well developed for wavelengths  $\geq 2\ \mu\text{m}$  or bulky. The most effective solution is to use a superluminescent diode (SLD) as a III–V gain chip and well mature Si-photonics for programmable wavelength selection.<sup>10</sup> A SLD offers a broad spectral emission, similar to a light emitting diode (LED), and a good beam quality, similar to a laser diode (LD). Such SLDs ensure single transverse mode operation, hence being favorable to integrate with Si photonics circuits, enabling the realization of programmable wavelength selection circuitry for multiple gas sensing.

The semiconductor light sources are well mature for wavelength below  $2\ \mu\text{m}$ , while their performance above  $2\ \mu\text{m}$  is quite limited mainly due to the lack of high quality gain-material. The standard material platforms such as InP experience a performance deterioration at a  $2\ \mu\text{m}$  wavelength, while limited research has been done on other narrow bandgap materials like GaInAsSb with emission wavelength up to almost  $4\ \mu\text{m}$ . The best results for  $2\ \mu\text{m}$  InP based SLDs at room temperature (RT) are reported to be 30 mW continuous wave (CW) output power, with a spectral full width at half maximum (FWHM) of 41 nm.<sup>11</sup> On the other-hand, the  $1.9\ \mu\text{m}$  single-pass GaSb SLDs demonstrated a maximum CW power up to 60 mW at RT.<sup>12</sup>

Here, we report a high performance double-pass GaSb-based SLD emitting at  $\sim 2\ \mu\text{m}$  under both CW and pulse current injection. At RT and CW operation, the SLD produced an output power up to 120 mW around  $2\ \mu\text{m}$ , which is about double compared to that of previously reported GaSb SLDs around this wavelength.<sup>12</sup> This improvement in the power can be related to the double-pass light amplification that allows high gain, but exposes the SLD to a risk of lasing or ringing in the case of small feedback obtained from facets. To keep the spectrum free from Fabry–Pérot resonances at high gain conditions, a cavity suppression (CS) element was added on the tilt facet of the SLD. The pulsed operation of the same device produced the

current source limited peak power up to 300 mW at RT for a 3 A injection current.

The devices were fabricated by solid source molecular beam epitaxy on n-GaSb substrates. Two compressively strained 10 nm thick Ga(0.78)In(0.22)Sb quantum wells (QWs) were embedded between lattice matched undoped 130 nm thick Al(0.3)Ga(0.7)AsSb waveguides (WGs). A 20 nm barrier consisting of the WG material was grown between the QWs. The gain waveguide structure was embedded within 2- $\mu\text{m}$  thick lattice matched Al(0.5)Ga(0.5)AsSb claddings. The closest 500 nm of the cladding on both sides of the WG was gradually doped to reduce the amount of free carriers overlapping with the waveguide mode. Beryllium was used for the p-type doping on the top side of the structure and tellurium for the n-type doping on the bottom side.

To suppress the laser oscillations in a cavity, an effective approach is to utilize a tilted ridge waveguide geometry.<sup>13,14</sup> In this work, we employed a “J-shape” waveguide layout, where the front-facet of ridge waveguide (RWG) is tilted at an angle  $\alpha$  to reduce the optical feedback and the rear-facet is kept straight to provide reflection for double-pass.<sup>15</sup> The advantage of this design is to double the effective gain length without altering the real waveguide size. Consequently, the net gain increase adds to the output power in SLD devices. The schematic of the SLD used in this work is shown in Fig. 1. In our design, we added an unpumped cavity suppression (CS) waveguide section at the front-facet of the RWG.<sup>12</sup> The optical mode in this section expands with the propagation distance, and after being reflected from the front-facet, it overlaps with the optical mode in RWG. By increasing the CS section length, this overlap decreases and the effective reflection of the mode in RWG reduced. Moreover, the light emitted out in this section spreads laterally, which prevents the absorption to saturate.<sup>16</sup> Additionally, the rear and front facets were coated with high-reflectivity ( $R > 92\%$  from 1.9  $\mu\text{m}$  to 2.05  $\mu\text{m}$ ) and low-reflectivity ( $R < 0.5\%$  from 1.9  $\mu\text{m}$  to 2.05  $\mu\text{m}$ ) coatings, respectively.

We studied the design by simulating the fraction of reflected fundamental transverse electric (TE) mode into the bent RWG at different tilt angles. The simulation results for different lengths of the CS section are shown in Fig. 2. The results reveal the tilt angles enabling minimum reflection for each CS section length. It is clear from simulation that longer CS sections are not effective in further reducing the mode reflection and they may also increase the undesired propagation losses. A CS section length of 150  $\mu\text{m}$  is sufficient to reduce the reflection to  $\sim 10^{-5}$ , which with anti-reflection (AR) coatings is further reduced to  $< 10^{-7}$ . In this simulation, we have ignored the absorption in the CS region, as the gain peak is red-shifted at high injection currents due to self-heating of the active region. To reduce the bend losses, we designed the bend section of the SLD following the Euler spiral

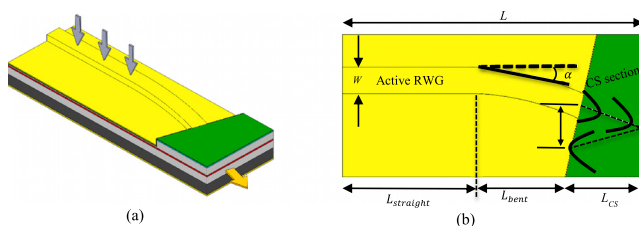


FIG. 1. (a) 3D view of the proposed SLD with the CS section and (b) 2D schematic with important device parameters.

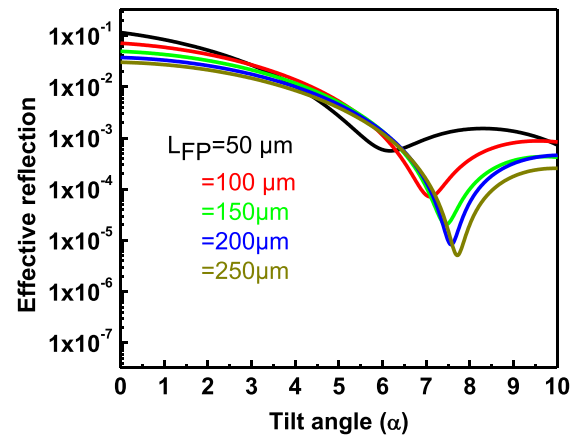


FIG. 2. Simulated power reflectivity of a tilted SLD for a fundamental TE mode at different tilt angles and CS section length.

approach,<sup>17</sup> where a bend waveguide is divided into multiple sections with a constant angle and a linearly increasing radius of curvature. In our SLDs, the bend radii are large enough to consider the bending losses to be negligible. The important SLD design parameters used in this study are listed in Table I.

Tested devices were operated under both CW and pulsed (500 ns pulse width, 5% duty cycle) current injection. The geometrical parameters of the tested device are shown in Table I. The measured light-current (L-I) curve and the emission spectra are shown in Figs. 3 and 4. We have found that CW output power deteriorates rapidly with increasing temperature due to increased junction temperature that promotes carrier leakage and nonradiative Auger recombination.<sup>18</sup> For CW operation, we achieved a maximum power of 120 mW (thermal limited), which is a two times increase compared to the current state-of-the-art GaSb SLDs at this wavelength.<sup>12</sup> For pulsed operation, we achieved a peak power of 300 mW (current limited). The emission spectrum of the SLD was measured using a Yokogawa AQ6375 optical spectrum analyzer with a 0.1 nm resolution. Figure 4 shows the spectra of the measured SLD in both CW and pulsed current injection. The tested devices demonstrate an amplified spontaneous emission with no obvious lasing sign in the entire drive current range. The spectral modulation depth is recorded to be less than  $< 14\%$  at maximum output power. The maximum power spectral density in CW, calculated as the maximum output power (120 mW) divided by the corresponding  $e^{-2}$  spectral width (67 nm), was 1.8 mW/nm. This is about

TABLE I. SLD design parameters.

$L$ ( $\mu\text{m}$ )	Total length of the device	3000
$L_{\text{straight}}$ ( $\mu\text{m}$ )	Length of straight RWG	1500
$L_{\text{bent}}$ ( $\mu\text{m}$ )	Length of bent RWG	1350
$L_{\text{FP}}$ ( $\mu\text{m}$ )	Length of the free propagation section	150
$R$ ( $\mu\text{m}$ )	Bent radius	18 000
$\alpha$ ( $^\circ$ )	Tilt angle	7.5
$w$ ( $\mu\text{m}$ )	Ridge width	5
$n_{\text{eff}}$	Effective index of a fundamental TE mode	3.498

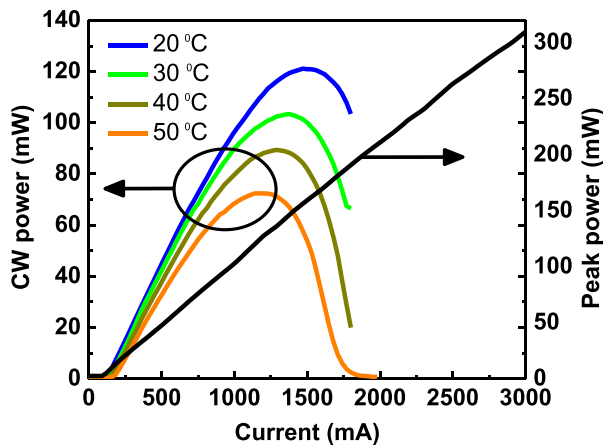


FIG. 3. L-I curve of a  $2\ \mu\text{m}$  SLD under CW operation and pulse injection. 500 ns pulse width, 5% duty cycle.

four times higher compared to GaSb SLDs in the same wavelength region.<sup>12</sup> The insets in Fig. 4 show a change in the peak wavelength and FWHM with injection current. The redshift in the peak wavelength with current is due to the carrier heating effect, which causes bandgap shrinkage. This supports our previous claim that absorption in the CS section is minimum at high current densities. An increase in the spectral FWHM with current can be attributed to a large material gain bandwidth<sup>19</sup> and pronounced junction heating in CW operation. The junction heating in CW operation causes thermal excitation of electrons to higher energy states. We observed that the red shift in the peak wavelength with current is reduced under pulse operation due to less average junction heating. Similarly, an increase in the FWHM under pulse operation is less pronounced than CW. We attribute this difference to a reduced junction heating, which in turn reduces the thermal excitation of electrons to high-energy states. This increase in the FWHM and redshift can be used as an opportunity to tune the SLD spectrum from  $\sim 1900\ \text{nm}$  to above  $\sim 2000\ \text{nm}$ . The spectral dips in Fig. 4(b) are due to the absorption of air molecules at shorter wavelengths.

The slow axis far-field (FF) pattern of the J-shaped SLD measured under CW is shown in Fig. 5. The FF profile fits well with the Gaussian profile without any side lobes. The inset in Fig. 5 shows the stability of slow axis FF divergence with injection current. The fast axis FF remains stable with the Gaussian profile across the entire current

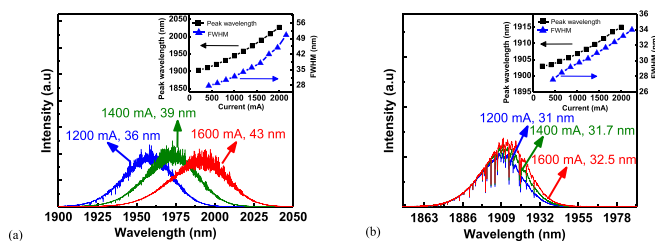


FIG. 4. (a) Spectra of a  $2\ \mu\text{m}$  SLD for different CW injection currents; (b) spectra of a  $2\ \mu\text{m}$  SLD under different pulse injection currents with 500 ns pulse width, 5% duty cycle. Each arrow indicates the current and spectral full width at half maximum. The inset shows the effect of current on the peak emission wavelength (square) and spectral FWHM (triangle).

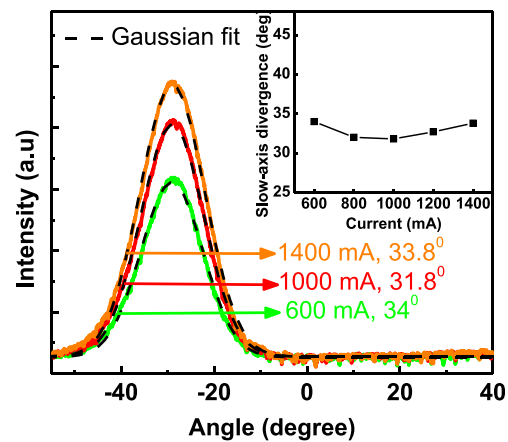


FIG. 5. Injection current dependence of the slow axis FF profile of a j-shaped SLD. Solid lines represent the measured FFs and the dashed lines are the corresponding Gaussian fits. Each arrow represents an injection current and a FF divergence. The inset in the figure shows the effect of current injection on slow axis FF divergence. Divergence is measured at  $e^{-2}$  of the maximum FF intensity.

range, and its divergence was measured to be  $63^\circ$ . These features are advantageous for fiber coupling of the SLD or its integration with Si-photonics waveguides. The decrease in slow axis FF divergence with current (shown as the inset of Fig. 5) is due to a decrease in the current dependent refractive index,<sup>20,21</sup> which broadens the near field. However, the reason for the increase in FF divergence for  $>1\ \text{A}$  current injection is not yet clear. We expect that this could be due to thermal lensing in the CS-section. The angle shift in the measured slow axis FF of the SLD can be confirmed accurately from Snell's law and Table I, i.e.,  $\sin^{-1}(3.498 \times \sin(7.5)) \approx 27^\circ$ .

In conclusion, an electrically pumped CW and pulsed high-power SLD using type-I GaInSb/GaSb compressively strained quantum wells is demonstrated. Using a J-shaped RWG, with a cavity-suppression element for double-pass amplification, a two fold increase in the output power is reported compared to the state-of-the-art results in this wavelength range. In particular, an output power up to 120 mW under CW RT operation and a peak power of about 300 mW for pulsed operation are reported. An increase in the injection current shifts the peak wavelength from 1900 nm to 2027 nm and the corresponding spectral FWHM from 28 nm to 50 nm. The SLD produced the maximum CW power spectral density of about 1.8 mW/nm. The far-field measurement of the SLD shows excellent beam with no side lobes.

The authors wish to thank MSc. Jarno Reuna for preparation of AR/HR coatings and Miss Mariia Bister for wafer level fabrication. The authors also wish to acknowledge the funding from European Union Horizon 2020 project MIREGAS "Programmable multiwavelength mid-IR source for gas sensing," Contract No. 644192. N. Zia likes to thank Tampere University for Graduate school funding. This work is also part of the Academy of Finland Flagship Programme PREIN #320168.

## REFERENCES

- L. S. Rothman, I. E. Gordon, A. Barbe, D. C. Benner, P. F. Bernath, M. Birk, V. Boudon, L. R. Brown, A. Campargue, J.-P. Champion *et al.*, "The HITRAN

- 2008 molecular spectroscopic database,” *J. Quant. Spectrosc. Radiat. Transfer* **110**, 533 (2009).
- <sup>2</sup>X. Chao, J. B. Jeffries, and R. K. Hanson, “Absorption sensor for CO in combustion gases using 2.3  $\mu\text{m}$  tunable diode lasers,” *Meas. Sci. Technol.* **20**, 115201 (2009).
- <sup>3</sup>M. E. Webber, R. Claps, F. V. Englich, F. K. Tittel, J. B. Jeffries, and R. K. Hanson, “Measurements of  $\text{NH}_3$  and  $\text{CO}_2$  with distributed-feedback diode lasers near 2.0  $\mu\text{m}$  in bioreactor vent gases,” *Appl. Opt.* **40**, 4395–4403 (2001).
- <sup>4</sup>H. Herbin, N. Picqué, G. Guelachvili, E. Sorokin, and I. T. Sorokina, “ $\text{N}_2\text{O}$  weak lines observed between 3900 and 4050  $\text{cm}^{-1}$  from long path absorption spectra,” *J. Mol. Spectrosc.* **238**, 256–259 (2006).
- <sup>5</sup>M. E. Webber, J. Wang, S. T. Sanders, D. S. Baer, and R. K. Hanson, “In situ combustion measurements of CO,  $\text{CO}_2$ ,  $\text{H}_2\text{O}$  and temperature using diode laser absorption sensors,” *Proc. Combust. Inst.* **28**(1), 407–413 (2000).
- <sup>6</sup>J. A. Gupta, P. J. Barrios, J. Lapointe, G. C. Aers, and C. Storey, “Single-mode 2.4  $\mu\text{m}$  InGaAsSb/AlGaAsSb distributed feedback lasers for gas sensing,” *Appl. Phys. Lett.* **95**(4), 041104 (2009).
- <sup>7</sup>B. G. Lee, M. A. Belkin, R. Audet, J. MacArthur, L. Diehl, C. Pflügl, F. Capasso, D. C. Oakley, D. Chapman, A. Napoleone, D. Bour, S. Corzine, G. Höfler, and J. Faist, “Widely tunable single-mode quantum cascade laser source for mid-infrared spectroscopy,” *Appl. Phys. Lett.* **91**(23), 231101 (2007).
- <sup>8</sup>L. A. Coldren, “Monolithic tunable diode lasers,” *IEEE J. Sel. Top. Quantum Electron.* **6**(6), 988–999 (2000).
- <sup>9</sup>U. H. Jacobs, K. Scholle, E. Heumann, G. Huber, M. Rattunde, and J. Wagner, “Room-temperature external cavity GaSb-based diode laser around 2.13  $\mu\text{m}$ ,” *Appl. Phys. Lett.* **85**, 5825 (2004).
- <sup>10</sup>P. Karioja, T. Alajoki, M. Cherchi, J. Ollila, M. Harjanne, N. Heinilehto, S. Suomalainen, N. Zia, H. Tuorila, J. Viheriälä, M. Guina, R. Buczyński, R. Kasztelaniec, T. Salo, S. Virtanen, P. Kluczyński, L. Borgen, M. Ratajczyk, and P. Kalinowski, “Multi-wavelength mid-IR light source for gas sensing,” *Proc. SPIE* **10110**, 101100P-1 (2017).
- <sup>11</sup>D. Wang, J. Zhang, C. Hou, Y. Zhao, F. Cheng, X. Jia, S. Zhai, N. Zhuo, J. Liu, F. Liu, and Z. Wang, “High performance continuous-wave InP-based 2.1  $\mu\text{m}$  superluminescent diode with InGaAsSb quantum well and cavity structure suppression,” *Appl. Phys. Lett.* **113**(16), 161107 (2018).
- <sup>12</sup>N. Zia, J. Viheriälä, R. Koskinen, A. Aho, S. Suomalainen, and M. Guina, “High power (60 mW) GaSb-based 1.9  $\mu\text{m}$  superluminescent diode with cavity suppression element,” *Appl. Phys. Lett.* **109**(23), 231102 (2016).
- <sup>13</sup>G. A. Alphonse, “Design of high-power superluminescent diodes with low spectral modulation,” *Proc. SPIE* **4648**, 125–139 (2002).
- <sup>14</sup>G. A. Alphonse and M. Toda, “Mode coupling in angled facet semiconductor optical amplifiers and superluminescent diodes,” *J. Lightwave Technol.* **10**(2), 215–219 (1989).
- <sup>15</sup>J.-H. Liang, T. Maruyama, Y. Ogawa, S. Kobayashi, J. Sonoda, H. Urae, S. Tomita, Y. Tomioka, and S. Kon, “High-power high-efficiency superluminescent diodes with J-shaped ridge waveguide structure,” in 14th Indium Phosphide and Related Materials Conference (Cat. No.02CH37307), Stockholm, Sweden (2002), pp. 119–122.
- <sup>16</sup>N. S. K. Kwong, K. Y. Lau, and N. Bar-Chaim, “High power high-efficiency GaAlAs superluminescent diodes with an internal absorber for lasing suppression,” *IEEE J. Quantum Electron.* **25**, 696–704 (1989).
- <sup>17</sup>M. Cherchi, S. Ylinen, M. Harjanne, M. Kapulainen, and T. Aalto, “Dramatic size reduction of waveguide bends on a micron-scale silicon photonic platform,” *Opt. Express* **21**, 17814–17823 (2013).
- <sup>18</sup>T. D. Eales, I. P. Marko, B. A. Ikyo, A. R. Adams, S. Arafin, S. Sprengel, M.-C. Amann, and S. J. Sweeney, “Wavelength dependence of efficiency limiting mechanisms in type-I mid-infrared GaInAsSb/GaSb lasers,” *IEEE J. Sel. Top. Quantum Electron.* **23**, 1–9 (2017).
- <sup>19</sup>J. Park and X. Li, “Theoretical and numerical analysis of superluminescent diodes,” *J. Lightwave Technol.* **24**(6), 2473 (2006).
- <sup>20</sup>G. P. Agrawal and N. K. Dutta, *Semiconductor Lasers* (Van Nostrand, New York, 1993).
- <sup>21</sup>L. Redaelli, H. Wenzel, M. Martens, S. Einfeldt, M. Kneissl, and G. Tränkle, “Index antiguiding in narrow ridge-waveguide (In,Al)GaN-based laser diodes,” *J. Appl. Phys.* **114**(11), 113102 (2013).